

DNA interaction studies of pyrazolone- and diimine-incorporated Mn(II), Co(II), Ni(II), Cu(II), and Zn(II) complexes: synthesis, spectroscopic characterization, and antimicrobial study

Arunagiri Sakthivel · Natarajan Raman ·
Livi Mitu

Received: 20 April 2012 / Accepted: 29 August 2012 / Published online: 23 October 2012
© Springer-Verlag 2012

Abstract Mn(II), Co(II), Ni(II), Cu(II), and Zn(II) mixed-ligand complexes were synthesized using 4-[(furan-2-ylmethylene)amino]-1,2-dihydro-1,5-dimethyl-2-phenyl-3*H*-pyrazol-3-one as the main ligand and 1,10-phenanthroline/2,2'-bipyridine as co-ligand(s). They were characterized by the usual analytical and spectral techniques. The data obtained reveal that the complexes adopt an octahedral geometry around the central metal ions. These complexes were found to be better antimicrobial agents than the free ligands. The DNA (CT) binding properties of the complexes were explored by UV–Vis, viscosity measurements, cyclic voltammetry, differential pulse voltammetry, and molecular docking studies. Binding constants for the above complexes were found to be on the order of 10^4 , indicating that most of the synthesized complexes are partial intercalators. The DNA-cleavage activities of the complexes were also assessed using supercoiled pUC19 DNA and gel electrophoresis, and the results revealed that the hydroxyl radical is likely to be the reactive species responsible for the cleavage of pUC19 DNA by the synthesized complexes.

Keywords Metal complex · DNA binding · Molecular docking · DNA cleavage · Antimicrobial activity

Introduction

Schiff bases are very attractive and have achieved recognition for their roles in biological processes such as mutagenesis and carcinogenesis. In addition to this, in recent years, lots of research have been done on the coordination chemistry of transition metal complexes with Schiff base ligands in order to mimic the physical and chemical behavior seen in biological processes [1, 2]. The interactions of transition metal complexes with DNA have been the focus of recent investigations. Metal complexes that exhibit interactions with DNA have been studied with the aim of developing probes for nucleic acid structures and chemotherapy agents [3]. By changing the ligand environment, it is possible to study the DNA binding and cleavage abilities of metal complexes. Such studies are also important for determining the mechanism of metal ion toxicity [4, 5].

The transition metal complexes of 1,2-dihydro-1,5-dimethyl-2-phenyl-3*H*-pyrazol-3-one (4-aminoantipyrine) and its derivatives have been extensively examined due to their wide range of applications in biological, analytical, and therapeutic fields [6]. Furfural is an important nontoxic compound. It is used as a fungicide and nematicide [7]. Hence, we elected to use this heterocyclic compound when attempting to design a Schiff base ligand with 4-aminoantipyrine. This ligand is useful as it contains aromatic rings that are able to stack the bases in DNA, oxygen and nitrogen atoms which can establish hydrogen bonds with DNA, and there is the possibility that the metal complexes

Electronic supplementary material The online version of this article (doi:10.1007/s00706-012-0857-7) contains supplementary material, which is available to authorized users.

A. Sakthivel · N. Raman (✉)
Research Department of Chemistry, VHNSN College,
Virudhunagar, Tamil Nadu 626 001, India
e-mail: drn_raman@yahoo.co.in

L. Mitu
Department of Physics and Chemistry, University of Pitetsi,
Pitetsi 110040, Romania

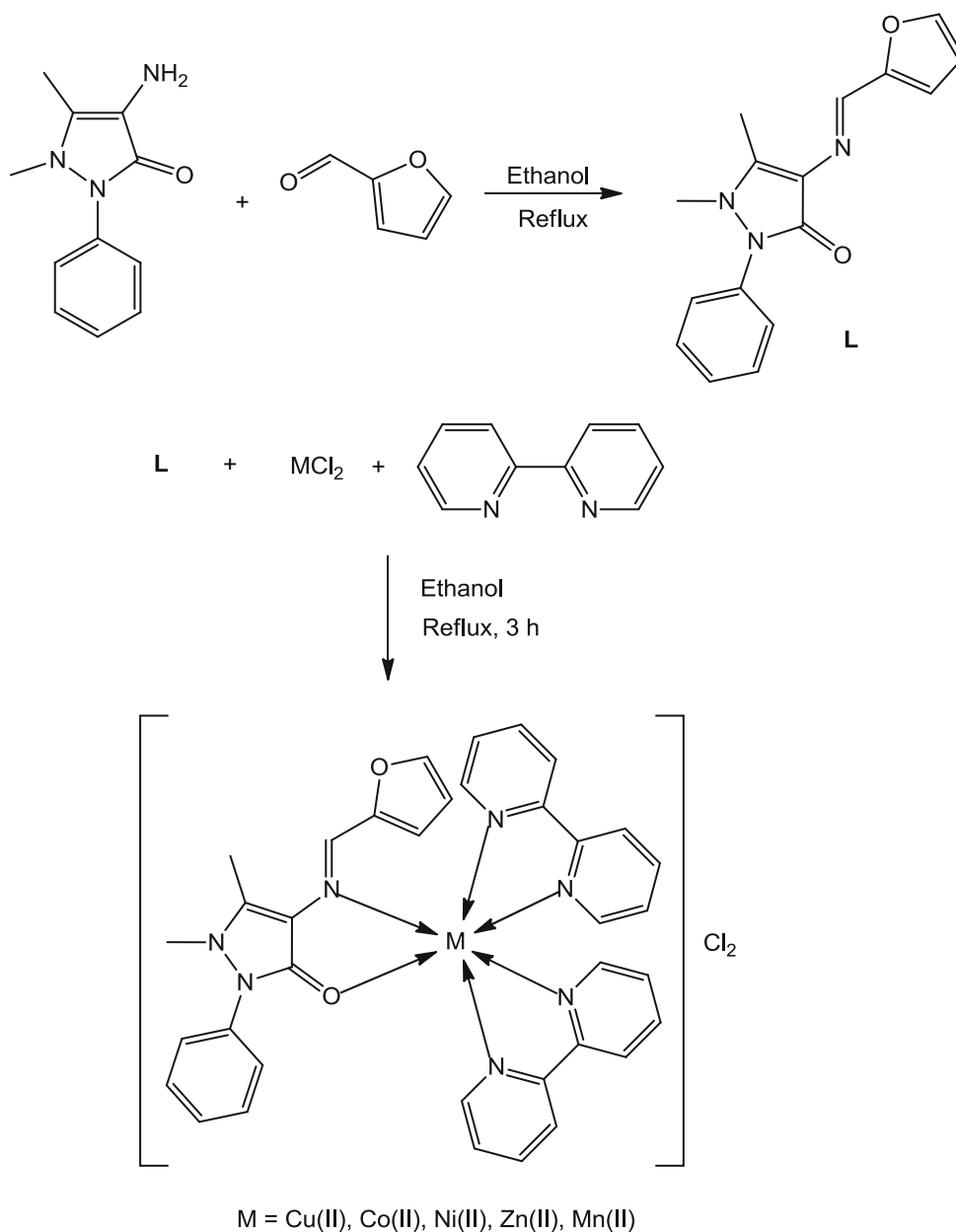
display a positive charge in order to interact electrostatically with the phosphate groups of DNA. In general, metal complexes that are capable of abstracting ribosyl hydrogen are expected to oxidize guanine or other nucleobases [8–10]. Current efforts are being made to design transition metal complexes that can be used as chemical nucleases in plasmid nicking or in direct strand scission. The practical use of transition metal complexes as chemical nucleases has also been documented [11, 12]. DNA binding, cleavage, and the antimicrobial activities of Mn(II), Co(II), Ni(II), Cu(II), and Zn(II) complexes that are derived from furfural with 4-aminoantipyrine and 1,10-phenanthroline

(phen)/2,2'-bipyridine (bpy) are of interest to us in our studies, as discussed in this present paper.

Results and discussion

Synthetic routes for the preparation of different compounds are depicted in Scheme 1. The ligand L and the complexes were found to be stable in air. L is soluble in common organic solvents but the complexes are soluble only in DMF and DMSO. The elemental analysis data on L and the complexes are in good agreement with the presented

Scheme 1



formulae. Physicochemical and spectroscopic studies indicate the formation of monomeric complexes of stoichiometry $[M(L)(phen/bpy)_2]Cl_2$ [13].

Infrared spectra

The IR spectra of the complexes were compared with the ligands in order to ascertain the changes that might have taken place. Although the Schiff base L and bpy/phen mixed-ligand complexes contain different types of C=N bonds arising from the bpy/phen ring and azomethine linkage, they are not well resolved in the spectra of the complexes [14, 15]. Furthermore, in the spectrum of L, although the azomethine $-CH=N$ band is superimposed on that of the C=O group of the imide, it is only a weak band. The peaks that appear in the range $1,639-1,600\text{ cm}^{-1}$ may be due to stretching of the azomethine $-CH=N$ group, whereas the bands in the range $1,552-1,541\text{ cm}^{-1}$ could be due to the $\nu(C=N)$ stretches of bpy/phen. The $\nu(C=O)$ band from L at $1,655\text{ cm}^{-1}$ is shifted in frequency by $\sim 10\text{ cm}^{-1}$ on complexation [16, 17]. A shift in the frequency of the band due to HC=N cannot be observed because it is not well resolved in the infrared spectra of the ligand and the complexes. However, the HC=N present in L is also involved in the formation of a bond with the metal atom during complexation, as clearly confirmed by the NMR data. The change in the frequency of the C=N band by 10 cm^{-1} indicates that bpy/phen rings are involved in the formation of the complex. Moreover, after coordination, the bands observed at around $881-892\text{ cm}^{-1}$ in bpy, $847-871\text{ cm}^{-1}$ in phen, $735-750\text{ cm}^{-1}$ (C-H_{def}), and $1,471-1,480\text{ cm}^{-1}$ and $1,315-1,325\text{ cm}^{-1}$ (C-N stretching bands) prove that the bpy and phen rings are coordinated to the metal ion through nitrogen. The new bands observed in the regions $418-442$ and $478-490\text{ cm}^{-1}$ for all of the complexes were assigned to M-N and M-O stretching vibrations, respectively, confirming the metal coordination [18, 19].

Molar conductivity

The high molar conductivities of the complexes in 10^{-3} M DMF solution reveal that they are electrolytic in nature, implying that the chloride anion is not coordinated to the central metal ion. The presence of a counter chloride ion was confirmed by Volhard's test.

Magnetic moments and electronic spectra

The free Schiff base ligand L exhibits two intense bands at $35,211$ and $27,777\text{ cm}^{-1}$ which are due to $\pi-\pi^*$ and $n-\pi^*$ transitions, respectively. In all metal complexes, the absorption bands at $31,055-34,602$ and $27,778-24,937\text{ cm}^{-1}$,

which are due to $\pi-\pi^*$ and $n-\pi^*$ transitions, exhibit blueshifts or redshifts due to the coordination of the ligand with metal ions. The electronic absorption spectral data for the ligand and all of the complexes are given in Table 1. The electronic spectra of the complexes $[Cu(L)(phen)_2]Cl_2$ and $[Cu(L)(bpy)_2]Cl_2$ exhibit one broad band at $15,760$ and $13,755\text{ cm}^{-1}$, respectively, with a low-intensity hump assigned to the $^2E_g \rightarrow ^2T_{2g}$ transition. The above data reveal that the Cu(II) complexes adopt a distorted octahedral geometry around the central metal ion. The observed magnetic moments of the complexes (1.93 and 1.82 BM , respectively) at room temperature indicate uncoupled mononuclear complexes of a magnetically diluted d^9 system with an $s = 1/2$ spin state of distorted octahedral geometry [20]. The monomeric nature of the complexes is further supported by microanalytical data and mass spectral data. The electronic spectra of the complexes $[Co(L)(phen)_2]Cl_2$ and $[Co(L)(bpy)_2]Cl_2$ show three broad bands in the visible region ($10,813$, $10,989$, $27,778$ and $10,111$, $11,248$, $24,937\text{ cm}^{-1}$, respectively), which were assigned to $^4T_{1g}(F) \rightarrow ^4T_{2g}(F)$, $^4T_{1g}(F) \rightarrow ^4A_{2g}(F)$, and $^4T_{1g}(F) \rightarrow ^4T_{2g}(P)$. These data reveal that the complexes have octahedral geometries. The observed magnetic moments of the cobalt(II) complexes at room temperature indicate that these complexes are monomeric. This is further supported by microanalytical data. The electronic spectra of the complexes $[Ni(L)(phen)_2]Cl_2$ and $[Ni(L)(bpy)_2]Cl_2$ show three low-intensity bands in the visible region around $10,977$, $10,040$, $27,732$ and $11,248$, $10,060$, $25,125\text{ cm}^{-1}$, which were assigned to $^3A_{2g}(F) \rightarrow ^3T_{2g}(F)$, $^3A_{2g}(F) \rightarrow ^3T_{1g}(F)$, and $^3A_{2g}(F) \rightarrow ^3T_{1g}(P)$ transitions, respectively, suggesting an octahedral geometry around the Ni(II) ion. The observed magnetic moments of the Ni(II) complexes (3.09 and 3.14 BM , respectively) at room temperature indicate uncoupled mononuclear complexes of a diluted d^8 system with an $s = 1$ spin state of octahedral geometry [21, 22]. The monomeric nature of the nickel complexes is further proven by their microanalytical data. The electronic spectra of the complexes $[Mn(L)(phen)_2]Cl_2$ and $[Mn(L)(bpy)_2]Cl_2$ show four broad, low-intensity bands in the visible region at around $15,478$, $24,331$, $27,732$, $29,700$ and $14,705$, $26,954$, $27,397$, $29,325\text{ cm}^{-1}$, respectively, which were assigned to $^6A_{1g} \rightarrow ^4T_{1g}$, $^6A_{1g} \rightarrow ^4T_{2g}(G)$, $^6A_{1g} \rightarrow ^4E_g$, $^6A_{1g} \rightarrow ^4T_{2g}(D)$ transitions. The electronic spectral data suggest an octahedral geometry around the Mn(II) ion. The observed magnetic moments of the Mn(II) complexes ($5.1-5.4\text{ BM}$) at room temperature indicate that these are monomeric complexes with octahedral geometries [23]. This is further supported by microanalytical data. The electronic absorption spectra for the diamagnetic Zn(II) complexes show bands in the region $34,602-29,498\text{ cm}^{-1}$ which were assigned to intraligand charge-transfer transitions [24].

Table 1 Electronic absorption spectral data for the synthesized compounds at 300 K

Compound	Solvent	Absorption/cm ⁻¹	Band assignment	Geometry
L	DMF	35,211 27,777	INCT INCT	–
[CuL(phen) ₂]Cl ₂	DMF	15,760 33,898	$E_g^2 \rightarrow T_{2g}$ INCT	Distorted octahedral
[CuL(bipy) ₂]Cl ₂	DMF	13,755 31,055	$^2E_g^2 \rightarrow T_{2g}$ INCT	Distorted octahedral
[CoL(phen) ₂]Cl ₂	DMF	10,813 10,989 27,778	$^4T_{1g}(F) \rightarrow ^4T_{2g}(F)$ $^4T_{1g}(F) \rightarrow ^4A_{2g}(F)$ $^4T_{1g}(F) \rightarrow ^4T_{2g}(P)$	Octahedral
[CoL(bpy) ₂]Cl ₂	DMF	10,111 11,248 24,937	$^4T_{1g}(F) \rightarrow ^4T_{2g}(F)$ $^4T_{1g}(F) \rightarrow ^4A_{2g}(F)$ $^4T_{1g}(F) \rightarrow ^4T_{2g}(P)$	Octahedral
[NiL(phen) ₂]Cl ₂	DMF	10,977 10,040 27,732	$^3A_{2g}(F) \rightarrow ^3T_{2g}(F)$ $^3A_{2g}(F) \rightarrow ^3T_{1g}(F)$ $^3A_{2g}(F) \rightarrow ^3T_{1g}(P)$	Octahedral
[NiL(bpy) ₂]Cl ₂	DMF	11,248 10,060 25,125	$^3A_{2g}(F) \rightarrow ^3T_{2g}(F)$ $^3A_{2g}(F) \rightarrow ^3T_{1g}(F)$ $^3A_{2g}(F) \rightarrow ^3T_{1g}(P)$	Octahedral
[MnL(phen) ₂]Cl ₂	DMF	15,748 24,331 27,732 29,700	$^6A_{1g} \rightarrow ^4T_{1g}$ $^6A_{1g} \rightarrow ^4T_{2g}(G)$ $^6A_{1g} \rightarrow ^4E_g$ $^6A_{1g} \rightarrow ^4T_{2g}(D)$	Octahedral
[MnL(bpy) ₂]Cl ₂	DMF	14,705 26,954 27,397 29,325	$^6A_{1g} \rightarrow ^4T_{1g}$ $^6A_{1g} \rightarrow ^4T_{2g}(G)$ $^6A_{1g} \rightarrow ^4E_g$ $^6A_{1g} \rightarrow ^4T_{2g}(D)$	Octahedral
[ZnL(phen) ₂]Cl ₂	DMF	33,783 29,498	INCT INCT	Octahedral
[ZnL(bpy) ₂]Cl ₂	DMF	34,602	INCT	Octahedral

Nuclear magnetic resonance spectra

The ¹H NMR spectra of the ligand L and the zinc complexes were recorded in DMSO-*d*₆. The ¹H NMR spectrum of the Schiff base ligand shows signals at δ = 2.4 and 3.1 ppm for C–CH₃ and N–CH₃ protons of the 4-aminoantipyrine moiety. It also shows signals at 6.63, 6.95, and 7.84 ppm for the furfuryl moiety and at 6.96, 7.35, and 7.38 ppm for the phenyl group of the 4-aminoantipyrine moiety. The azomethine proton (CH=N) is observed at 9.54 ppm. The ¹H NMR spectrum of the Schiff base ligand is given in the Electronic supplementary material (ESM). The signals for the azomethine proton (–CH=N) of the bpy and phen mixed-ligand zinc complexes are shifted upfield, to 9.34 and 9.41 ppm, respectively, compared to the free ligand (9.54 ppm), suggesting the coordination of the azomethine group with the metal ion. The zinc complex [Zn(L)(bpy)₂]Cl₂ (Fig. 1) shows additional resonance peaks at 7.67, 8.20, and 8.62 ppm, which were assigned to bpy protons. Similarly, the additional resonance peaks

observed at 8.0, 8.25, 8.45, and 8.86 ppm in the spectrum of the complex [Zn(L)(phen)₂]Cl₂ (see the ESM) were assigned to phen protons. There is no appreciable change in the other signals of the complex [18].

The ¹³C NMR spectrum of L shows aromatic carbons at 112.06–143.19 ppm. The signals from the C=O and C=N carbons of ligand L observed at 159 and 163 ppm are shifted upfield to 153 and 160 ppm for the bpy mixed-ligand Zn(II) complex and to 152.9 and 159.5 ppm for the phen mixed-ligand Zn(II) complex (see the ESM). There are no appreciable changes in the other peaks.

Mass spectra

The FAB mass spectra of synthesized L and the [Mn(L)(bpy)₂]Cl₂ complexes were recorded and the molecular ion peaks obtained confirm the proposed formulae. The mass spectrum of L shows an M + 1 peak at *m/z* = 282 (91.71 %) corresponding to the (C₁₆H₁₅N₃O₂)⁺ ion. Also, the spectrum exhibits fragments at *m/z* = 214,

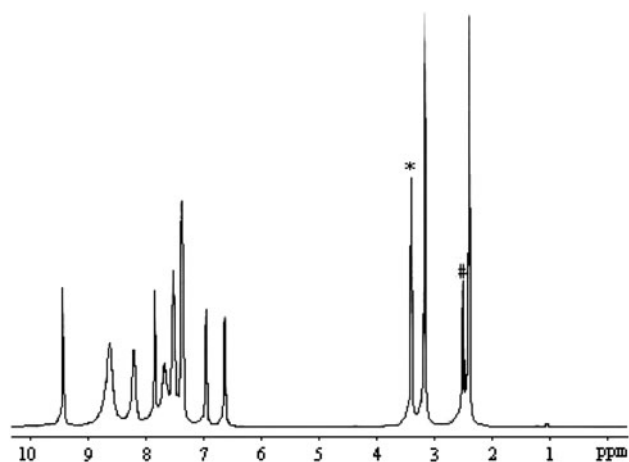


Fig. 1 ^1H NMR spectrum of the $[\text{Zn}(\text{L})(\text{bpy})_2]\text{Cl}_2$ complex in $\text{DMSO-}d_6$ (hash and asterisk indicate peaks from the DMSO solvent and trace water, respectively)

202, 188, 173, and 157 corresponding to $[\text{C}_{12}\text{H}_{12}\text{N}_3\text{O}]^+$, $[\text{C}_{11}\text{H}_{11}\text{N}_3\text{O}]^+$, $[\text{C}_{11}\text{H}_{11}\text{N}_2\text{O}]^+$, $[\text{C}_{10}\text{H}_8\text{N}_2\text{O}]^+$, and $[\text{C}_{10}\text{H}_8\text{N}_2]^+$, respectively (Fig. 2a). The mass spectrum of $[\text{Mn}(\text{L})(\text{bpy})_2]^{2+}$ shows peaks at $m/z = 648$ and 649 with abundances of 20 and 15 %, respectively. The peak at $m/z = 648$ may represent the molecular ion peak of the complex, and the other peak is an isotopic species (Fig. 2b). The strongest peaks (base peaks) at $m/z = 281$, 157, and 95 represent the stable species $(\text{C}_{16}\text{H}_{15}\text{N}_3\text{O}_2)^+$, $(\text{C}_{10}\text{H}_8\text{N}_2)^+$, and $(\text{C}_5\text{H}_4\text{NO})^+$, respectively. The m/z of the molecular ion peak confirms that the stoichiometry of the complexes is of the $[\text{ML}(\text{bpy})_2]\text{Cl}_2$ type. This is further supported by the mass spectra of all the complexes.

The observed peaks are in good agreement with their empirical formulae as indicated by microanalytical data. Similarly, the DART-MS spectrum was recorded for the $[\text{Co}(\text{L})(\text{phen})_2]\text{Cl}_2$ complex (see the ESM). The strongest peak (base peak) at $m/z = 181$ represents the stable $[\text{C}_{12}\text{H}_8\text{N}_2]^+$ moiety (i.e., the phen ligand). Moreover, the spectrum exhibits fragments at $m/z = 702$, 422, and 282 corresponding to $[\text{CoC}_{40}\text{H}_{31}\text{O}_2\text{N}_7]^+$, $[\text{Co}(\text{C}_{12}\text{H}_8\text{N}_2)_2]^+$, and $[\text{C}_{16}\text{H}_{15}\text{N}_3\text{O}_2]^+$, respectively. These represent the $[\text{Co}(\text{L})(\text{phen})_2]\text{Cl}_2$ complex after the removal of the two chloride ions, the $\text{Co}(\text{phen})_2$ moiety, and L, respectively. Similarly, the other fragments are also in good agreement with the proposed structure of the complex. Thus, the mass spectral data confirm the stoichiometry of the complex as $[\text{CoL}(\text{X})_2]\text{Cl}_2$ (where L = ligand, X = phen). The mass spectral data of other complexes also support the above stoichiometry. This stoichiometry is further supported by the elemental data, which are in close agreement with the values calculated from molecular formulae assigned to these complexes. Thus, the mass spectral data reinforce the conclusion drawn from the analytical and conductance values.

Electron paramagnetic resonance spectra

To obtain further information about the stereochemistry and the site of the metal–ligand bonding, and to determine the magnetic interactions in the metal complexes, EPR studies of all the copper(II) complexes were carried out. The spectra of the complexes were recorded in powder and also in DMSO solution at 300 K (room temperature) and 77 K (liquid nitrogen temperature, LNT). However, the $[\text{Cu}(\text{L})(\text{bpy})_2]\text{Cl}_2$ complex in the frozen state shows four well-resolved peaks with low intensities in the low-field region and one intense peak in the high-field region (Fig. 3). The spin Hamiltonian parameters and bonding parameters were calculated and are summarized in Tables 2 and 3, respectively. The EPR spectrum of $[\text{Cu}(\text{L})(\text{phen})_2]\text{Cl}_2$ at both 300 and 77 K shows one intense absorption band in the high-field region, and is isotropic due to tumbling motion of the molecules (see the ESM) as well as dipolar exchange and unresolved hyperfine interaction in the solid state. The magnetic moment calculated from the equation $\mu_{\text{eff}} = g[s(s+1)]^{1/2}$ using the experimental g_{iso} value (2.14) agrees very well with the measured magnetic susceptibility range of 1.93 BM, indicating that the solid structure is retained in DMSO solution. The EPR spectrum of the copper complex at 77 K indicates a poorly resolved nitrogen super hyperfine structure (Fig. 3) in the perpendicular region due to the interaction of the odd Cu(II) electron with nitrogen atoms. The magnetic susceptibility value reveals that the copper complex has a magnetic moment of 1.93 BM, corresponding to one unpaired electron, indicating that the complex is mononuclear.

In the present case, Cu(II) complexes measured in DMSO at LNT gave the following values: $g_{\parallel} = 2.2728$, $g_{\perp} = 2.0665$ for $[\text{Cu}(\text{L})(\text{phen})_2]\text{Cl}_2$; $g_{\parallel} = 2.2721$, $g_{\perp} = 2.0536$ for $[\text{Cu}(\text{L})(\text{bpy})_2]\text{Cl}_2$. For both complexes, the g_{\parallel} and g_{\perp} values were greater than 2.04, consistent with copper(II) in axial symmetry with all the principal axes aligned parallel. These g values indicate an elongated tetragonally distorted octahedral stereochemistry [25]. However, the observation $g_{\parallel} > g_{\perp} > g_e$ shows that the unpaired electron is in the $d_{x^2-y^2}$ orbital of the Cu(II) ion [26]. The values of the g factors are used to determine the geometric parameter G , representing a measure of the exchange interaction between Cu(II) centers in a polycrystalline compound, using the formula $G = (g_{\parallel} - 2.0023)/(g_{\perp} - 2.0023)$ [27]. If $G < 4$, there is an exchange interaction between the Cu(II) centers, while if $G > 4$, the exchange interaction is negligible. The present copper complexes have G values greater than 4 indicating exchange interaction is either absent or very little in the solid complexes.

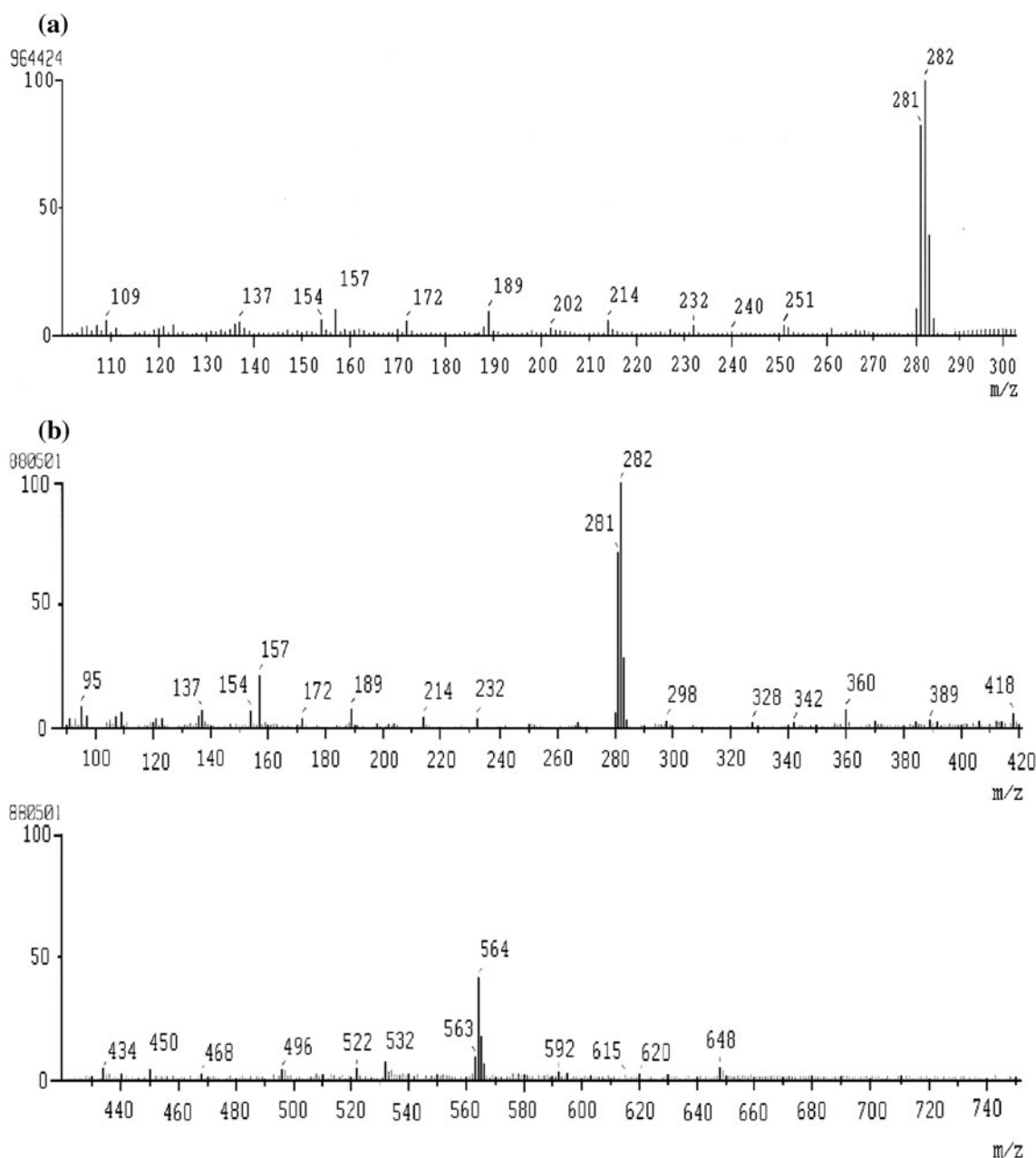


Fig. 2 FAB mass spectra of ligand L (a) and the complex $[\text{Mn}(\text{L})(\text{bpy})_2]\text{Cl}_2$ (b)

The EPR parameters g_{\parallel} , g_{\perp} , A_{II} and the $d-d$ transition energies are used to evaluate the bonding parameters α^2 , β^2 , and γ^2 , which may be regarded as measures of the covalency of the in-plane σ bonds, in-plane π bonds, and out-of-plane π bonds. α^2 can be calculated using the equation:

$$\alpha^2 = \left(\frac{A_{\parallel}}{P} \right) + (g_{\parallel} - 2.0023) + \frac{3}{7}(g_{\perp} - 2.0023) + 0.04.$$

If α^2 is 0.5, it indicates pure covalent bonding, while $\alpha^2 = 1.0$ suggests pure ionic bonding. In the present case, α^2 is 0.6430 for $[\text{Cu}(\text{L})(\text{phen})_2]\text{Cl}_2$ and 0.6506

for $[\text{Cu}(\text{L})(\text{bpy})_2]\text{Cl}_2$, which indicate that both of these complexes have some covalent character. The out-of-plane π -bonding (γ^2) and in plane π -bonding (β^2) parameters were calculated using the following expressions:

$$\beta^2 = (g_{\parallel} - 2.0023)E / (-8\lambda\alpha^2)$$

$$\gamma^2 = (g_{\perp} - 2.0023)E / (-2\gamma\alpha^2).$$

In these equations, $\lambda = -828 \text{ cm}^{-1}$ for the free metal ion, and the E values for the complexes $[\text{Cu}(\text{L})(\text{phen})_2]\text{Cl}_2$ and $(\text{Cu}(\text{L})(\text{bpy})_2)\text{Cl}_2$ are 15,760 and 13,755 cm^{-1} ,

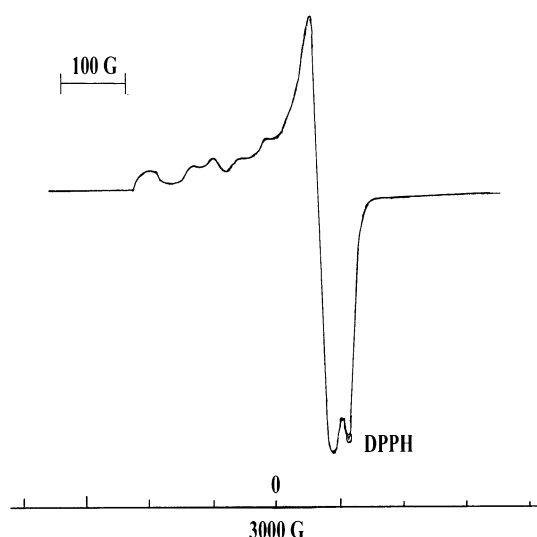


Fig. 3 The X-band EPR spectrum of the $[\text{Cu}(\text{L})(\text{bpy})_2]\text{Cl}_2$ complex in DMSO at 77 K

respectively. The observed values for $[\text{Cu}(\text{L})(\text{phen})_2]\text{Cl}_2$ ($\beta^2 = 0.999$ and $\gamma^2 = 0.944$) and for $[\text{Cu}(\text{L})(\text{bpy})_2]\text{Cl}_2$ ($\beta^2 = 0.8629$ and $\gamma^2 = 0.6498$) indicate that there is an interaction in the out-of-plane π -bonding whereas the in-plane π -bonding is completely ionic. This is further confirmed by orbital reduction factors, which can be estimated using the following relations:

$$K_{\parallel}^2 = [(g_{\parallel} - 2.0023)\Delta E]/8\lambda_0$$

$$K_{\perp}^2 = [(g_{\perp} - 2.0023)\Delta E]/8\lambda_0,$$

where λ_0 is the spin orbit coupling constant for the copper(II) ion (-828 cm^{-1}). K_{\parallel} and K_{\perp} are the parallel and perpendicular components of the orbital reduction factor (K). Significant information about the nature of bonding in the copper(II) complex can be derived from the relative magnitudes of K_{\parallel} and k_{\perp} . In the case of pure σ -bonding, $K_{\parallel} \approx k_{\perp}$, whereas $K_{\parallel} < k_{\perp}$ implies considerable in-plane

π -bonding, while $K_{\parallel} > k_{\perp}$ for out-of-plane π -bonding. For the present case, the observed order is K_{\parallel} (0.6426) $>$ k_{\perp} (0.1518) for $[\text{Cu}(\text{L})(\text{phen})_2]\text{Cl}_2$ and K_{\parallel} (0.5594) $>$ k_{\perp} (0.1057) for $[\text{Cu}(\text{L})(\text{bpy})_2]\text{Cl}_2$, implying a greater contribution from out-of-plane π -bonding than from in-plane π -bonding to metal–ligand π -bonding. Thus, the spectral data discussed above confirm the proposed structures of the ligand L and the complexes (Scheme 1).

DNA binding studies: electronic spectra

Adding increasing amounts of calf thymus (CT) DNA to all complexes results in a decrease in the molar absorption (hypochromism) of the π - π^* absorption band as well as a redshift of a few nm (1–2 nm), indicating the binding of the complexes to DNA in different modes in different extents. The binding of an intercalative complex molecule to DNA has been well characterized to produce notable hypochromism and a significant redshift due to a strong stacking interaction between the aromatic chromophore of the ligand and DNA base pairs, with the degree of hypochromism and the size of the redshift linked to the strength of the intercalative interaction [28–30]. The magnitudes of the hypochromism and the redshift observed for all of the phen mixed-ligand complexes are higher than those seen for the bpy mixed-ligand complexes (shown in Table 4). The observed binding is typical of classical intercalators and partially intercalating metal complexes bound to CT DNA. A quantitative comparison of the DNA-binding affinities of the complexes was performed using the following equation:

$$[\text{DNA}]/(\varepsilon_a - \varepsilon_f) = [\text{DNA}]/(\varepsilon_b - \varepsilon_f) + 1/K_b(\varepsilon_b - \varepsilon_f),$$

where $[\text{DNA}]$ is the concentration of DNA in base pairs, ε_a is the apparent extinction coefficient obtained by calculating $A_{\text{obs}}/[\text{complex}]$, ε_f corresponds to the extinction coefficient of the complex in its free form, and ε_b refers to

Table 2 The spin Hamiltonian parameters of copper complexes in DMSO solution at 300 and 77 K

Complex	Hyperfine constant/ 10^{-4} cm^{-1}			g_{\parallel}	g_{\perp}	g_{iso}
	A_{\perp}	A_{\parallel}	A_{iso}			
$[\text{CuL}(\text{phen})_2]\text{Cl}_2$	125	110	120	2.2728	2.0665	2.1353
$[\text{CuL}(\text{bpy})_2]\text{Cl}_2$	85	120	98	2.2721	2.0536	2.1264

Table 3 The EPR bonding parameters of copper complexes in DMSO solution

Complex	α^2	β^2	γ^2	G	K_{\parallel}	K_{\perp}	K
$[\text{CuL}(\text{phen})_2]\text{Cl}_2$	0.6430	0.9994	0.9443	4.1023	0.6426	0.1518	0.3154
$[\text{CuL}(\text{bpy})_2]\text{Cl}_2$	0.6506	0.8629	0.6498	5.0765	0.5594	0.1057	0.2569

Table 4 Absorption spectral properties of the synthesized complexes with DNA

Complexes	λ_{\max}/nm		$\Delta\lambda/\text{nm}$	H/%	$K_b/10^4 \text{ M}^{-1}$ ^a
	Free	Bound			
[CuL(bpy) ₂]Cl ₂	311.5	311.4	0.1	9.06	1.84
[CuL(phen) ₂]Cl ₂	384	378.0	6.0	7.40	2.50
[CoL(bpy) ₂]Cl ₂	341.0	338.7	2.3	20.40	1.85
[CoL(phen) ₂]Cl ₂	338.5	339.8	1.3	24.80	3.78
[NiL(bpy) ₂]Cl ₂	340.1	339.5	0.6	8.30	4.79
[NiL(phen) ₂]Cl ₂	339.0	339.7	0.7	29.14	9.52
[ZnL(bpy) ₂]Cl ₂	339.5	339.7	0.2	12.70	2.38
[ZnL(phen) ₂]Cl ₂	365.4	360.6	4.8	26.0	2.93
[MnL(bpy) ₂]Cl ₂	342.0	340.9	1.1	22.0	0.94
[MnL(phen) ₂]Cl ₂	340.5	340.9	0.4	18.85	2.31

^a Error limit: $\pm 5\%$

the extinction coefficient of the complex in the bound form. A straight line is obtained when $[\text{DNA}]/(\varepsilon_a - \varepsilon_f)$ versus $[\text{DNA}]$ is plotted. The slope of the straight line is equivalent to $1/(\varepsilon_b - \varepsilon_f)$ and the y intercept is equivalent to $1/K_b(\varepsilon_b - \varepsilon_f)$. The value of K_b (the binding constant) was determined from the ratio of the slope to the intercept.

The intrinsic binding constants K_b for $[\text{M}(\text{L})(\text{phen})_2]^{2+}$ are greater than those for $[\text{M}(\text{L})(\text{bpy})_2]^{2+}$, suggesting that the diimine rather than the 4-(furfurylideneamino)antipyrine face of each complex is involved in DNA binding, and that coordinated phen and bpy rings are engaged in partial insertion in between the base pairs of DNA. The observed K_b values are much lower than those observed for typical classical intercalators (EthBr, $K_b = 1.4 \times 10^6 \text{ M}^{-1}$ in 25 mM Tris-HCl/40 mM NaCl buffer, pH 7.2). Hence, it is obvious that the present complexes are involved in weaker intercalative interactions, in spite of the steric clash between the 4-(furfurylideneamino)antipyrine ligand and the DNA double helix. Generally, the mixed-ligand complex offers the variation in geometry, size, hydrophobicity, and hydrogen-bonding ability which are the major factors to determine the DNA binding affinity [31]. Here, the ligand is not expected to be flat with the phenyl group; it may be twisted out of the plane of phenanthroline. Further, its lack of planarity diminishes the favorability of the ligand for intercalation, while the diimine part of the complex enhances the stacking of the diimine with the DNA base pairs. Further, the small binding constant values may indicate surface aggregation and groove binding rather than any interaction with the DNA base pairs. It is also notable that compounds exhibiting low binding constants have been identified in the literature as intercalating agents [32]. The electronic absorption spectrum of $[\text{Mn}(\text{L})(\text{bpy})_2]\text{Cl}_2$ in the absence and presence of increasing amounts of DNA is given in Fig. 4, and the phen complex is shown in the ESM.

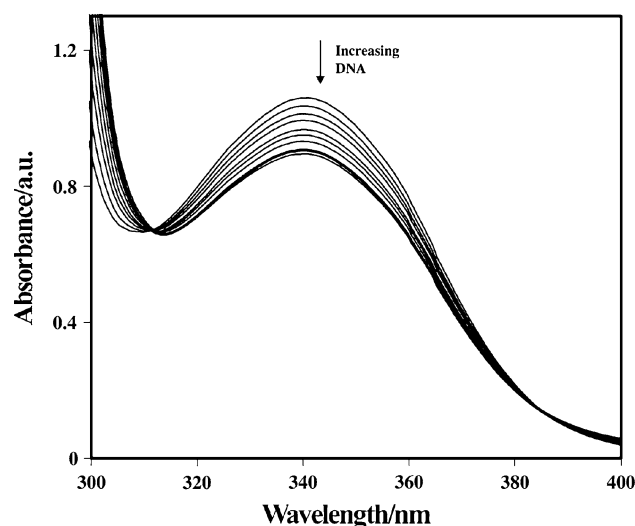


Fig. 4 Absorption spectra of $[\text{Mn}(\text{L})(\text{bpy})_2]\text{Cl}_2$ in the presence of increasing amounts of DNA ($[\text{complex}] = 50 \mu\text{M}$, $[\text{DNA}] = 25\text{--}125 \mu\text{M}$ from top to bottom) in Tris-HCl buffer. The arrow indicates the change in absorbance upon increasing the DNA concentration

From Table 4, we can infer that the Ni(II) complexes interact with DNA to the greatest degree, with binding constants K_b of $4.79 \times 10^4 \text{ M}^{-1}$ and $9.52 \times 10^4 \text{ M}^{-1}$, respectively. These values are very distinctive of metal-based compounds that bind to DNA via intercalation. This is because the nickel complexes enhance the oxidation of guanine residues in DNA [33–35]. This has been experimentally proven through DNA cleavage studies, as described later in this manuscript. Moreover, this distinct mechanism causes the nickel complexes to tend to act as effective intercalators and artificial nucleases when compared to other members.

Viscosity measurements

Measuring the viscosity of DNA is regarded as the least ambiguous and most critical test of a DNA binding model in solution, and affords stronger arguments for an intercalative DNA binding mode [36, 37]. The viscosity of DNA is significantly enhanced by complete or partial intercalation of complexes into the DNA base-pair stack, but it is slightly disturbed by the electrostatic or covalent binding of molecules [38]. To investigate the nature of DNA binding of the mixed-ligand complexes, viscosity measurements of CT DNA were carried out by varying the concentrations of the added complexes. The changes in the relative specific viscosity of CT DNA in the presence and absence of the complex were plotted against $1/R$ ($=[\text{complex}]/[\text{DNA}]$).

A classical intercalation mode causes a significant increase in the viscosity of DNA due to an increase in base-pair separation at intercalation sites and hence an increase

in the overall DNA length. In our study, the ability of each complex to increase the viscosity of DNA depended upon the diimine ligand. Phen insertion produces greater viscosity than insertion of the bpy ligand (as shown in the ESM). The results of this viscosity study agree well with the hypochromism and K_b values observed for the above complexes. Lengthening of the DNA duplex occurs upon the partial insertion of phen and the deeper insertion of bpy between the DNA base pairs.

Electrochemical studies

Cyclic and differential pulse voltammetric techniques are extremely useful for probing the nature and mode of the binding of metal complexes to DNA. Typical cyclic voltammograms obtained for the complex $[\text{Cu}(\text{L})(\text{bpy})_2]\text{Cl}_2$ in the absence and presence of varying amounts of DNA are shown in Fig. 5. The incremental addition of CT DNA to the complex causes the anodic and cathodic peak currents of the complex to decrease. This result shows that the complex stabilizes the duplex (GC pairs) by intercalation. The incremental addition of CT DNA to the complex causes a shift in the potential of the peaks in the cyclic voltammograms. The cathodic and anodic peaks both show positive or negative shifts, which indicates the intercalation of the complex into the base pairs of the DNA. If one of the peak shifts was positive and the other was negative, it would indicate that the complex intercalates into and electrostatically binds to the CT DNA, or that it breaks the secondary structure of the DNA.

In the differential pulse voltammogram of the complex $[\text{Cu}(\text{L})(\text{bpy})_2]\text{Cl}_2$ obtained in the absence and the presence of varying amounts of DNA (in which a significant

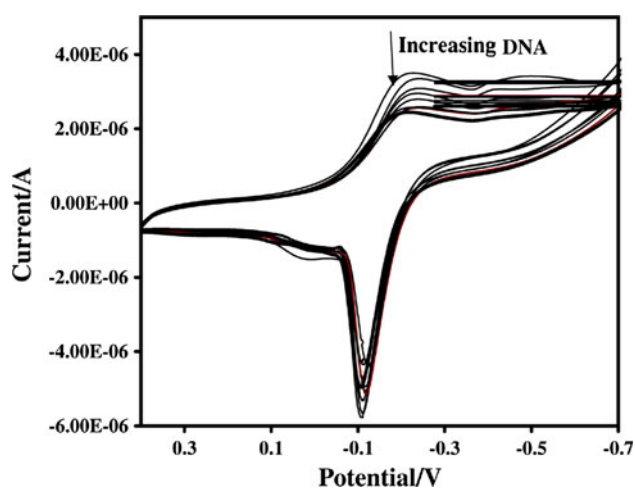


Fig. 5 Cyclic voltammogram (scan rate of 10 mV/s) of $[\text{Cu}(\text{L})(\text{bpy})_2]\text{Cl}_2$ in the absence and presence of increasing amounts of DNA: 10, 20, 40, 100, 150, 200, 250 μM . Supporting electrolyte: 5 mM Tris-HCl + 50 mM NaCl in water (pH 7.2)

decrease in current intensity with increasing DNA concentration is observed; see Fig. 6), the shift in potential is related to the ratio of the binding constants by the following equation:

$$E_b - E_f = 0.0591 \log(K_{[\text{red}]}/K_{[\text{ox}]})$$

where E_b and E_f are the peak potentials of the complex in its bound and free forms, respectively. In the present study, both the bpy and the phen mixed-ligand complexes exhibited one-electron transfer during the redox process, and the I_p_c/I_p_a value was less than unity, indicating that the reaction of the complex on the glassy carbon electrode surface was quasi-reversible. Other complexes—those including Co(II), Ni(II), Mn(II), and Zn(II)—show considerable shifts in both their cathodic and anodic peak potentials when CT DNA is added incrementally. Most of the complexes we synthesized exhibited both anodic and cathodic peak potential shifts which were either positive or negative, except for manganese complexes (Table 5). This indicates the mode of intercalation that occurs when the DNA binds with bpy/phen mixed-ligand Schiff base complexes. It is interesting to note that phen mixed-ligand complexes show a greater decrease in current intensity than bpy mixed-ligand complexes (Fig. 5 and the ESM). This observation suggests that the intercalative mode that occurs when DNA binds to phen mixed-ligand complexes is stronger than that involved when DNA binds to bpy mixed-ligand complexes. Another interesting aspect of our study is that manganese complexes exhibit positive and negative shifts in peak potential. This indicates that there is an intercalative and electrostatic binding mode between DNA and these complexes, or that they break up the secondary structure of DNA.

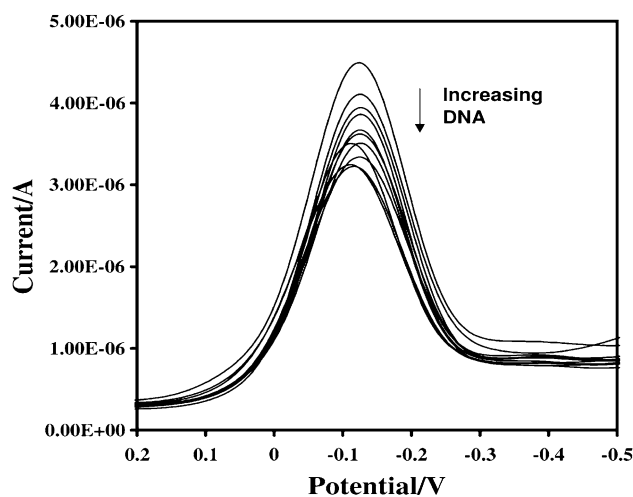


Fig. 6 Differential pulse voltammogram (scan rate of 10 mV/s) of 100 μM of the complex $[\text{Cu}(\text{L})(\text{bpy})_2]\text{Cl}_2$ in the absence and presence of increasing amounts of DNA: 10, 20, 40, 100, 150, 200, 250 μM . Supporting electrolyte: 5 mM Tris-HCl + 50 mM NaCl in water (pH 7.2)

Table 5 Electrochemical parameters for the interaction of DNA with metal(II) complexes

Complex	$E_{1/2}/V$		$\Delta E_p/V$		$K[\text{red}]/K[\text{ox}]$	I_{pc}/I_{pa}^a
	Free	Bound	Free	Bound		
[CuL(phen)Cl ₂]	-0.2303	-0.1068	-0.1205	-0.0031	3.2900	0.6782
[CuL(bpy)Cl ₂]	-0.1725	-0.1795	-0.1110	-0.1050	1.5959	0.6900
[CoL(phen) ₂ Cl ₂]	-0.7663	-0.7128	-0.0435	-0.1264	1.2294	4.0317
[CoL(bpy) ₂ Cl ₂]	0.1624	0.1887	0.0413	0.0706	0.7321	0.1660
[NiL(phen) ₂ Cl ₂]	-0.5878	-0.5625	0.0613	0.0326	1.3658	0.3615
[NiL(bpy) ₂ Cl ₂]	0.35025	0.3705	-0.0645	-0.0910	1.3658	0.4660
[ZnL(phen) ₂ Cl ₂]	-0.0438	-0.1289	-0.1136	0.2562	2.1797	0.4050
[ZnL(bpy) ₂ Cl ₂]	-0.8503	-0.9411	0.1177	0.1978	3.1930	6.3402
[MnL(phen) ₂ Cl ₂]	-0.6267	-0.4882	0.1098	-0.1985	4.0813	0.8319
[MnL(bpy) ₂ Cl ₂]	0.3150	0.3320	-0.0300	-0.0780	0.5362	0.8895

^a Error limit: $\pm 5\%$

Antimicrobial activity

The investigated compounds were tested for antimicrobial activity against bacteria and fungi. The minimum inhibitory concentration (MIC) values of the investigated compounds are summarized in Table 6 and 7. A comparative study of L and the complexes (in terms of MIC values) indicates that the complexes exhibit higher antimicrobial activities than the free ligand. From the MIC values, it is apparent that the phen mixed-ligand complexes are more potent than the other investigated complexes, which can be explained via Overtone's concept and Tweedy's chelation theory [39, 40]. These complexes also disturb the respiration process of the cell and thus block the synthesis of proteins that restrict further growth of the organism. Furthermore, the mode of action of the compound may involve the formation of a hydrogen bond through the azomethine group with the active center of the cell, resulting in interference with the normal cell process, and the metal complexes are generally more active than the

ligands because the metal complexes can serve as a vehicle for the activation of ligands—the principal cytotoxic species [41]. The 4-(furfurylideneamino)antipyrine Schiff base ligand may play an important role in this antimicrobial activity, as well as the presence of four imine groups brings the transformation reaction in biological systems. The activities of ligands and their complexes increase as the concentration increases, because it is a well-known fact that concentration plays a vital role in increasing the degree of inhibition. The results indicate that the complexes show more activity than the ligands against the same microorganisms under identical conditions (Tables 6, 7). These data are in good agreement with literature values [42].

It is well known that chelation is not the only criterion for antibacterial activity. Some important factors such as the nature of the metal ion, the nature of the ligand, the coordinating sites, the geometry of the complex, the concentration, hydrophilicity, lipophilicity, and the presence of co-ligands have a considerable influence on the antibacterial activity. Steric and pharmacokinetic factors undoubtedly also play a

Table 6 Minimum inhibitory concentrations (mg cm⁻³) of the synthesized compounds against the growth of four fungi

Compound	<i>Aspergillus niger</i>	<i>Fusarium solani</i>	<i>Curvularia lunata</i>	<i>Rhizoctonia bataicola</i>
L	26.2	27.4	25.5	24.9
[CuL(phen) ₂ Cl ₂]	13.7	15.9	13.5	16.5
[CuL(bpy) ₂ Cl ₂]	19.7	20.1	20.3	19.7
[CoL(phen) ₂ Cl ₂]	16.0	15.3	16.5	15.9
[CoL(bpy) ₂ Cl ₂]	21.0	21.2	21.3	20.4
[NiL(phen) ₂ Cl ₂]	17.1	18.7	16.2	17.5
[NiL(bpy) ₂ Cl ₂]	20.3	20.9	20.7	20.3
[ZnL(phen) ₂ Cl ₂]	16.5	16.8	16.9	17.7
[ZnL(bpy) ₂ Cl ₂]	20.5	19.6	19.0	19.6
[MnL(phen) ₂ Cl ₂]	16.9	16.0	17.0	15.9
[MnL(bpy) ₂ Cl ₂]	19.8	19.7	19.5	19.3
Nystatin	1.0	1.7	0.9	1.5

Table 7 Minimum inhibitory concentrations (mg cm^{-3}) of the synthesized compounds against the growth of four bacteria

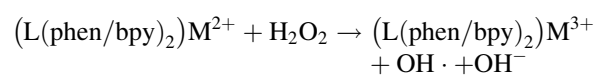
Compound	<i>S. aureus</i>	<i>B. subtilis</i>	<i>E. coli</i>	<i>K. pneumoniae</i>
L	21.7	20.9	28.0	29.6
[CuL(phen) ₂]Cl ₂	18.7	20.9	10.5	12.5
[CuL(bpy) ₂]Cl ₂	16.7	16.1	15.3	14.7
[CoL(phen) ₂]Cl ₂	12.0	13.3	11.5	13.9
[CoL(bpy) ₂]Cl ₂	17.0	18.2	16.3	16.4
[NiL(phen) ₂]Cl ₂	17.5	18.0	13.2	17.7
[NiL(bpy) ₂]Cl ₂	19.3	18.9	18.7	18.3
[ZnL(phen) ₂]Cl ₂	16.5	14.8	15.9	17.1
[ZnL(bpy) ₂]Cl ₂	18.5	19.6	17.0	17.6
[MnL(phen) ₂]Cl ₂	17.9	16.7	17.1	14.9
[MnL(bpy) ₂]Cl ₂	19.8	18.7	16.5	17.3
Streptomycin	1.7	2.3	1.3	2.0

decisive role in deciding the potency of an antimicrobial agent. The presence of lipophilic and polar substituents is expected to enhance antibacterial activity. Heterocyclic ligands with multifunctionality which have a greater chance of interacting with either nucleoside bases (even after complexation with a metal ion) or with biologically essential metal ions present in the biosystem may be promising candidates for bactericides since they always tend to interact (especially with a few enzymatic functional groups) in order to achieve higher coordination numbers [43]. Thus, the antibacterial property of metal complexes cannot be ascribed to chelation alone; it is a complicated blend of several contributions.

Cleavage of pUC19 DNA

The nuclease activity exhibited by certain transition metal complexes in the presence of hydrogen peroxide can be attributed to the participation of the hydroxyl radical in DNA cleavage. When nicked, the naturally occurring supercoiled circular form of pUC19 DNA (form I) gives rise to an open circular form (form II). Relatively fast migration is observed for form I, but rather slow migration for form II. In the present study, a DNA cleavage experiment was conducted at 35 °C in the presence and absence of H₂O₂. As can be seen from the results shown in Fig. 7a, the gel electrophoretic separation of plasmid pUC19 DNA occurs when treated with [ML(bpy)₂]Cl₂ complexes. Control experiments suggest that untreated DNA does not show any significant DNA cleavage (lane 1). However, in the presence of peroxide, most of the [ML(bpy)₂]Cl₂ and [ML(phen)₂]Cl₂ complexes convert the supercoiled plasmid DNA into a mixture of nicked (form II) and linear (form III) DNA (Fig. 7b and Fig. 7c). Further, in the presence of DMSO (4 mm³), [CuL(bpy)₂]Cl₂ + H₂O₂ does

not show any DNA-cleavage activity (lane 4 in Fig. 7b). In this case, the cleavage is inhibited by free-radical scavengers (DMSO), implying that hydroxyl radicals mediate the cleavage. This provides clear evidence for the involvement of hydroxyl radicals in the DNA strand scission performed by M(II) complexes. Here, the toxicity of metal is expressed through the formation of hydroxyl radical, which involves redox process with metal center and H₂O₂. Moreover, the mechanism commences with the oxidation of deoxyribose units by the free radicals, leading to the fragmentation of the sugar-phosphate backbone. The loaded (L(phen/bpy)₂)M²⁺ complexes damage DNA more efficiently in the presence of an oxidant and form DNA adducts that migrate at different rates. This can be attributed to the formation of hydroxyl free radicals. The production of a hydroxyl free radical in the reaction between the complex and the oxidant may occur as shown below:



These OH free radicals participate in the oxidation of the deoxyribose moiety, followed by the hydrolytic cleavage of the sugar-phosphate backbone. Here, the most significant shifts are observed for Co(II) and Ni(II) (Fig. 7b, lanes 7 and 5), whereas the DNA adducts with Cu(II) and Zn(II) complexes (lanes 3 and 8) migrate to a lesser extent. This difference in the migration patterns of the adducts points to a difference in the binding modes of these compounds compared to the other members of the series. Control experiments using DNA alone did not show any significant cleavage of pUC19 DNA, even after longer exposure times. Based on these results, we can conclude that the Ni(II) complexes (Fig. 7b, lane 5) loaded with H₂O₂ are most effective at cleaving DNA, and can thus be considered better artificial nucleases than the other members and the control. Hence, it is evident from the interactions of the complexes with CT DNA and pUC19 DNA that the cobalt and nickel complexes are more effective DNA-damaging agents than the other members. This is because the cobalt and nickel complexes enhance the oxidation of guanine residues in DNA [33–35]. This mechanism means that the cobalt and nickel complexes are more effective intercalators and artificial nucleases than the copper and zinc complexes.

Molecular docking analysis

The results of spectroscopic titration, viscosity, and cyclic voltammetry experiments suggest that Cu(II), Ni(II), Co(II), and Zn(II) complexes interact with DNA via intercalation. The binding constant values are in the range of 10⁴ per mole for all of the complexes, which indicates

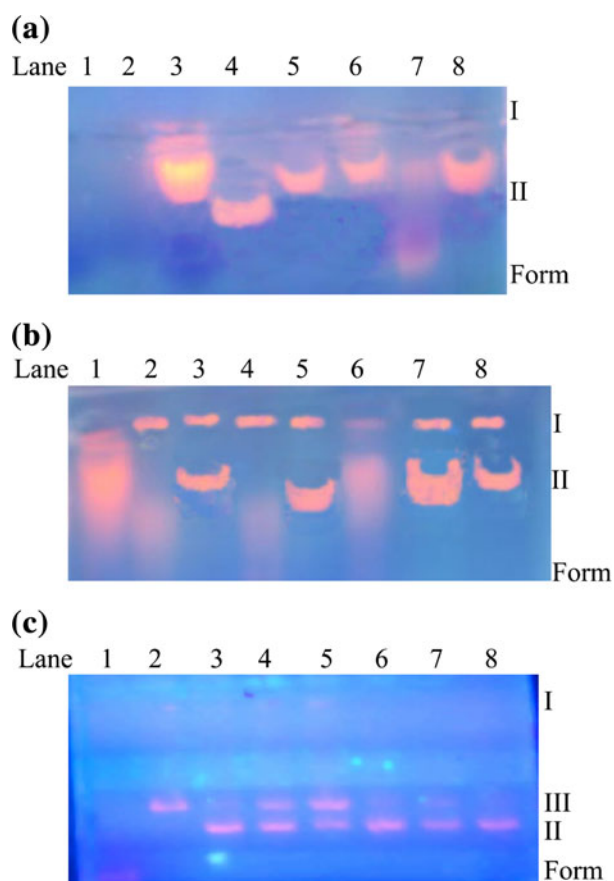


Fig. 7 **a** The gel electrophoretic separation of plasmid pUC19 DNA treated with $[M(L)(bpy)_2]Cl_2$ complexes. Lane 1 DNA marker, lane 2 DNA + ligand, lane 3 DNA + $[Ni(L)(bpy)_2]Cl_2$, lane 4 DNA + $[Co(L)(bpy)_2]Cl_2$, lane 5 DNA + $[Cu(L)(bpy)_2]Cl_2$, lane 6 DNA + $[Mn(L)(bpy)_2]Cl_2$, lane 7 DNA + $[Zn(L)(bpy)_2]Cl_2$. **b** The gel electrophoretic separation of plasmid pUC19 DNA treated with $[M(L)(bpy)_2]Cl_2$ complexes. Lane 1 DNA marker, lane 2 DNA + ligand, lane 3 DNA + $[Cu(L)(bpy)_2]Cl_2 + H_2O_2$, lane 4 DNA + $[Cu(L)(bpy)_2]Cl_2 + H_2O_2 + DMSO$, lane 5 DNA + $[Ni(L)(bpy)_2]Cl_2 + H_2O_2$, lane 6 DNA + $[Mn(L)(bpy)_2]Cl_2 + H_2O_2$, lane 7 DNA + $[Co(L)(bpy)_2]Cl_2 + H_2O_2$, lane 8 DNA + $[Zn(L)(bpy)_2]Cl_2 + H_2O_2$. **c** The gel electrophoretic separation of plasmid pUC19 DNA treated with $[M(L)(phen)_2]Cl_2$ complexes. Lane 1 DNA marker, lane 2 DNA + $[Cu(L)(phen)_2]Cl_2 + H_2O_2$, lane 3 DNA + $[Cu(L)(phen)_2]Cl_2$, lane 4 DNA + $[Co(L)(phen)_2]Cl_2 + H_2O_2$, lane 5 DNA + $[Ni(L)(phen)_2]Cl_2 + H_2O_2$, lane 6 DNA + $[Zn(L)(phen)_2]Cl_2 + H_2O_2$, lane 7 DNA + $[Mn(L)(phen)_2]Cl_2 + H_2O_2$, lane 8 DNA + ligand + H_2O_2

that these complexes may intercalate between the DNA base pairs. This is mainly due to effective stacking forces between the aromatic ligands and DNA bases. Docking experiments were performed in order to find the preferred binding site and orientation of the ligand inside the DNA. Docking experiments using the energy-minimized docked structures suggest that the best possible geometries of the metal complexes occur when they act as partial intercalators (as shown in Fig. 8). Structural analysis of the docked structures provides significant information on the binding patterns of these complexes. The binding energies of the

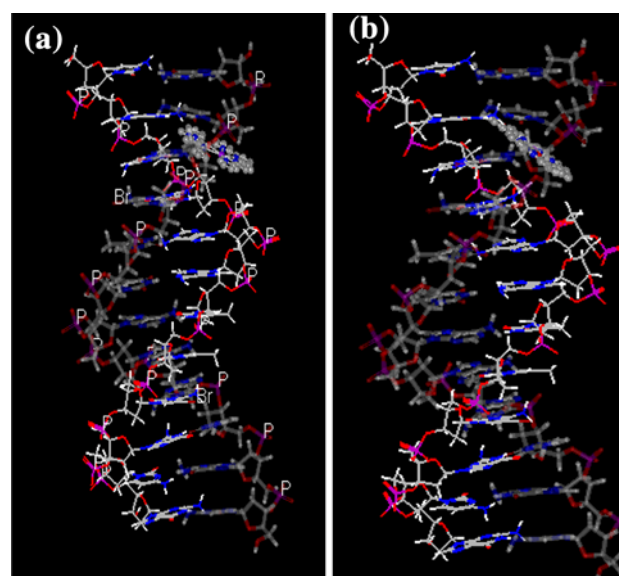


Fig. 8 Interaction of the complexes **a** $[Cu(L)(bpy)_2]Cl_2$ and **b** $[Cu(L)(phen)_2]Cl_2$ with d(CGCGAATTCGCG) strands of DNA via intercalation binding

docked metal complexes $[Cu(L)(phen)_2]Cl_2$, $[Cu(L)(bpy)_2]Cl_2$, $[Co(L)(phen)_2]Cl_2$, $[Co(L)(bpy)_2]Cl_2$, $[Ni(L)(phen)_2]Cl_2$, $[Ni(L)(bpy)_2]Cl_2$, $[Zn(L)(phen)_2]Cl_2$, $[Zn(L)(bpy)_2]Cl_2$, $[Mn(L)(phen)_2]Cl_2$, and $[Mn(L)(bpy)_2]Cl_2$ are -557.32 , -555.19 , -557.33 , -527.94 , -547.01 , -534.19 , -528.81 , -527.08 , -530.04 , and -529.36 kJ mol^{-1} , respectively, which correlate well with the corresponding experimental DNA binding values. It was found that the binding between the DNA and target molecules was stronger when the relative binding energy was more negative.

Conclusion

The synthesized L and the complexes were characterized by microanalytical data, IR, UV-Vis, 1H NMR, EPR, and mass spectra. The data show that the complexes are of type $[M(L)(phen/bpy)_2]Cl_2$. The UV-Vis, magnetic susceptibility, and EPR spectral data for the complexes suggest an octahedral geometry around the central metal ion. The complexes show high electrical conductance, indicating that these chelates are electrolytes. Their magnetic susceptibility values provide evidence for their monomeric nature. The planarity and flexible extended conjugation of the ligands have a strong effect on the DNA-binding and DNA-cleavage activities of these complexes. The intercalative binding of these complexes with DNA is supported by their electronic absorption spectra as well as cyclic voltammetry, difference pulse voltammetry, and viscometric studies. The planarity of the complexes increases their DNA-binding and DNA-cleavage activities. The

results obtained from in vitro antifungal and antibacterial tests show that all of these complexes possess potent antimicrobial activities toward bacteria and fungi. It was found that the activities of the complexes are higher than that of the free ligand.

Experimental

All reagents and chemicals were procured from Merck (Darmstadt, Germany). Solvents used for electrochemical and spectroscopic studies were purified by standard procedures [44]. DNA was purchased from Bangalore Genei (Bangalore, India). Agarose (molecular biology grade) and ethidium bromide (EB) were obtained from Sigma (St. Louis, MO, USA). Tris(hydroxymethyl)aminomethane-HCl (Tris-HCl) buffer solution was prepared using deionized, doubly distilled water. Carbon, hydrogen, and nitrogen analyses of the complexes were carried out on a CHN analyzer (1108, Heraeus Carlo Erba, Hanau, Germany). The IR spectra (KBr discs) of the samples were recorded in the range of 400–4,000 cm^{-1} on a PerkinElmer (Waltham, MA, USA) 783 series FTIR spectrophotometer. Electronic absorption spectra in the 200–1,100 nm range were obtained on a Shimadzu (Kyoto, Japan) UV-1601 spectrophotometer. *N,N*-dimethylformamide (DMF) was used as solvent when obtaining electronic spectra for both the ligand L and its complexes. The NMR spectra of L and the zinc complexes were recorded on a Bruker (Billerica, MA, USA) Avance DRX 300 FT-NMR spectrometer, using DMSO- d_6 as solvent, at the University Science Instrumentation Centre (USIC), Madurai Kamaraj University, Madurai, India. Tetramethylsilane was used as the internal standard. Fast atom bombardment mass spectra of the complexes were recorded on a JEOL (Tokyo, Japan) SX 102/DA-6000 mass spectrometer/data system using argon/xenon (6 kV, 10 mA) as the FAB gas. X-band EPR spectra of the copper complexes were recorded at RT (300 K) and LNT (77 K) using DPPH as the g-marker.

The molar conductances of the complexes (10^{-3} M) in DMF were measured at room temperature with a Deep Vision (Tamilnadu, India) model 601 digital direct reading deluxe conductivity meter. Magnetic susceptibility measurements were carried out using the Gouy method at room temperature on powdered samples of the complexes. $\text{CuSO}_4 \cdot 5\text{H}_2\text{O}$ was used as calibrant. Electrochemical measurements were performed on a CHI (Austin, TX, USA) 620C electrochemical analyzer with a three-electrode system comprising a glassy carbon electrode as the working electrode, a platinum wire as the auxiliary electrode, and Ag/AgCl as the reference electrode. Solutions were deoxygenated by purging with N_2 prior to measurements. The metal content of each complex was determined

according to a method described previously [45]. Chloride ion was determined gravimetrically as silver chloride [46]. The ligand L was synthesized by following the previously reported procedure [47]. The ligand was purified by column chromatography eluted with alcohol:DMF mixture and the purity was checked by TLC. The complexes were purified by repeated washing with ethanol.

Synthesis of $[M(L)(phen)_2]Cl_2$ and $[M(L)(bpy)_2]Cl_2$

The metal(II) complexes were prepared by mixing the appropriate molar quantities of the ligands and metal salts using the following procedure. An ethanolic solution of L (10 mmol) was heated under reflux with an ethanolic solution of the metal(II) chloride (10 mmol) for ca. 3 h. To the above mixture, an ethanolic solution of 1,10-phenanthroline/2,2'-bipyridine (20 mmol) was added, and the reflux was continued for ca. 1 h. The resulting solid product was filtered, washed with ethanol, and dried in vacuo.

[4-[(Furan-2-ylmethylene)amino]-1,2-dihydro-1,5-dimethyl-2-phenyl-3H-pyrazol-3-one]bis(1,10-phenanthroline)copper(II) chloride ($\text{C}_{40}\text{H}_{31}\text{Cl}_2\text{CuN}_7\text{O}_2$)
Yield: 62 %; IR (KBr): $\bar{\nu} = 1,647$ (C=O), 1,601 (–CH=N), 1,545 (C=N) cm^{-1} ; $\Lambda_m = 157.50$ S cm^2 mol^{-1} ; $\mu_{\text{eff}} = 1.93$ BM; UV–Vis (DMF): $\lambda_{\text{max}} = 15,760, 33,898$ cm^{-1} ; MS: $m/z = 741$ (M^+).

[4-[(Furan-2-ylmethylene)amino]-1,2-dihydro-1,5-dimethyl-2-phenyl-3H-pyrazol-3-one]bis(1,10-phenanthroline)cobalt(II) chloride ($\text{C}_{40}\text{H}_{31}\text{Cl}_2\text{CoN}_7\text{O}_2$)
Yield: 54 %; IR (KBr): $\bar{\nu} = 1,645$ (C=O), 1,597 (–CH=N), 1,547 (C=N) cm^{-1} ; $\Lambda_m = 138.96$ S cm^2 mol^{-1} ; $\mu_{\text{eff}} = 4.81$ BM; UV–Vis (DMF): $\lambda_{\text{max}} = 27,778, 10,989, 10,813$ cm^{-1} ; MS: $m/z = 736$ (M^+).

[4-[(Furan-2-ylmethylene)amino]-1,2-dihydro-1,5-dimethyl-2-phenyl-3H-pyrazol-3-one]bis(1,10-phenanthroline)nickel(II) chloride ($\text{C}_{40}\text{H}_{31}\text{Cl}_2\text{NiN}_7\text{O}_2$)
Yield: 59 %; IR (KBr): $\bar{\nu} = 1,647$ (C=O), 1,599 (–CH=N), 1,545 (C=N) cm^{-1} ; $\Lambda_m = 131.47$ S cm^2 mol^{-1} ; $\mu_{\text{eff}} = 3.09$ BM; UV–Vis (DMF): $\lambda_{\text{max}} = 27,732, 10,040, 10,977$ cm^{-1} ; MS: $m/z = 736$ (M^+).

[4-[(Furan-2-ylmethylene)amino]-1,2-dihydro-1,5-dimethyl-2-phenyl-3H-pyrazol-3-one]bis(1,10-phenanthroline)manganese(II) chloride ($\text{C}_{40}\text{H}_{31}\text{Cl}_2\text{MnN}_7\text{O}_2$)
Yield: 60 %; IR (KBr): $\bar{\nu} = 1,648$ (C=O), 1,591 (–CH=N), 1,547 (C=N) cm^{-1} ; $\Lambda_m = 144.46$ S cm^2 mol^{-1} ; $\mu_{\text{eff}} = 5.10$ BM; UV–Vis (DMF): $\lambda_{\text{max}} = 29,700, 27,732, 24,331, 15,748$ cm^{-1} ; MS: $m/z = 732$ (M^+).

[4-[(Furan-2-ylmethylene)amino]-1,2-dihydro-1,5-dimethyl-2-phenyl-3H-pyrazol-3-one]bis(1,10-phenanthroline)zinc(II) chloride (C₄₀H₃₁Cl₂N₇O₂Zn)
Yield: 57 %; IR (KBr): $\bar{\nu}$ = 1,646 (C=O), 1,597 (–CH=N), 1,548 (C=N) cm⁻¹; ¹H NMR (DMSO-*d*₆): δ = 2.40 (s, 3H, C–CH₃), 3.10 (s, 3H, N–CH₃), 6.63, 6.95 (m, 2H, furfuryl), 6.96–7.38 (m, 5H, phenyl), 7.84 (m, 1H, furfuryl), 8.00, 8.25, 8.45, 8.86 (m, 8H, phen), 9.41 (s, CH=N) ppm; ¹³C NMR (DMSO-*d*₆): δ = 9.7 (C–CH₃), 35.3 (N–CH₃), 112.2, 113.6, 116.2, 124.7, 125.5, 126.9, 128.8, 129.1, 134.4, 139.5, 139.8, 143.2, 145.1, 148.8, 151.7, 152.9 (C=O), 159.5 (HC=N) ppm; Λ_m = 136.86 S cm² mol⁻¹; μ_{eff} = 0 BM; MS: *m/z* = 743 (M⁺).

[4-[(Furan-2-ylmethylene)amino]-1,2-dihydro-1,5-dimethyl-2-phenyl-3H-pyrazol-3-one]bis(2,2'-bipyridine)copper(II) chloride (C₃₆H₃₁Cl₂CuN₇O₂)
Yield: 64 %; IR (KBr): $\bar{\nu}$ = 1,647 (C=O), 1,601 (–CH=N), 1,545 (C=N) cm⁻¹; Λ_m = 112.69 S cm² mol⁻¹; μ_{eff} = 1.82 BM; UV–Vis (DMF): λ_{max} = 31,055, 13,755 cm⁻¹; MS: *m/z* = 657 (M⁺).

[4-[(Furan-2-ylmethylene)amino]-1,2-dihydro-1,5-dimethyl-2-phenyl-3H-pyrazol-3-one]bis(2,2'-bipyridine)cobalt(II) chloride (C₃₆H₃₁Cl₂CoN₇O₂)
Yield: 61 %; IR (KBr): $\bar{\nu}$ = 1,648 (C=O), 1,599 (–CH=N), 1,545 (C=N) cm⁻¹; Λ_m = 132.45 S cm² mol⁻¹; μ_{eff} = 4.93 BM; UV–Vis (DMF): λ_{max} = 24,937, 11,248, 10,111 cm⁻¹; MS: *m/z* = 653 (M⁺).

[4-[(Furan-2-ylmethylene)amino]-1,2-dihydro-1,5-dimethyl-2-phenyl-3H-pyrazol-3-one]bis(2,2'-bipyridine)nickel(II) chloride (C₃₆H₃₁Cl₂N₇NiO₂)
Yield: 60 %; IR (KBr): $\bar{\nu}$ = 1,649 (C=O), 1,592 (–CH=N), 1,546 (C=N) cm⁻¹; Λ_m = 130.09 S cm² mol⁻¹; μ_{eff} = 3.14 BM; UV–Vis (DMF): λ_{max} = 25,125, 11,248, 10,060 cm⁻¹; MS: *m/z* = 652 (M⁺).

[4-[(Furan-2-ylmethylene)amino]-1,2-dihydro-1,5-dimethyl-2-phenyl-3H-pyrazol-3-one]bis(2,2'-bipyridine)manganese(II) chloride (C₃₆H₃₁Cl₂MnN₇O₂)
Yield: 58 %; IR (KBr): $\bar{\nu}$ = 1,647 (C=O), 1,602 (–CH=N), 1,543 (C=N) cm⁻¹; Λ_m = 152.70 S cm² mol⁻¹; μ_{eff} = 5.40 BM; UV–Vis (DMF): λ_{max} = 29,325, 27,397, 26,954, 14,705 cm⁻¹; MS: *m/z* = 649 (M⁺).

[4-[(Furan-2-ylmethylene)amino]-1,2-dihydro-1,5-dimethyl-2-phenyl-3H-pyrazol-3-one]bis(2,2'-bipyridine)zinc(II) chloride (C₃₆H₃₁Cl₂N₇O₂Zn)
Yield: 56 %; IR (KBr): $\bar{\nu}$ = 1,647 (C=O), 1,601 (–CH=N), 1,545 (C=N) cm⁻¹; ¹H NMR (DMSO-*d*₆): δ = 2.40 (s, 3H, C–CH₃), 3.10 (s, 3H, N–CH₃), 6.63, 6.95 (m, 2H, furfuryl), 6.96–7.38 (m, 5H, phenyl), 7.84 (m, 1H, furfuryl), 7.67, 8.20, 8.62 (m, 8H, bpy), 9.34 (s, 1H, CH=N) ppm; ¹³C NMR (DMSO-*d*₆): δ = 9.6 (C–CH₃), 35.1 (N–CH₃),

112.1, 113.3, 116.1, 124.6, 126.8, 129.0, 134.4, 139.9, 143.2, 144.9, 149.1, 151.6, 153.0 (C=O), 160.0 (HC=N) ppm; Λ_m = 123.18 S cm² mol⁻¹; μ_{eff} = 0 BM; MS: *m/z* = 659 (M⁺).

DNA-binding and DNA-cleavage experiments

All experiments involving the interaction of the complexes with calf thymus (CT) DNA were carried out in Tris–HCl buffer (50 mM Tris–HCl, pH 7.2) containing 5 % DMF at room temperature. A solution of CT DNA in the buffer gave a ratio of UV absorbances at 260 and 280 nm of about 1.89:1, indicating that the CT DNA was sufficiently free from protein [48]. The CT DNA concentration per nucleotide was determined by absorption spectroscopy using a molar absorption coefficient of 6,600 M⁻¹ cm⁻¹ at 260 nm [49].

An absorption titration experiment was performed by maintaining the concentration of the metal complex at 50 μ M while varying the concentration of CT DNA within 40–400 μ M. While measuring the absorption spectrum, equal quantities of CT DNA were added to both the complex solution and the reference solution to eliminate the absorbance of CT DNA itself. Using the absorption data, the intrinsic binding constant K_b was determined from a plot of [DNA]/($\epsilon_a - \epsilon_f$) versus [DNA] and the equation

$$[DNA] / (\epsilon_a - \epsilon_f) = [DNA] / (\epsilon_b - \epsilon_f) + [K_b(\epsilon_b - \epsilon_f)]^{-1}, \quad (1)$$

where [DNA] is the concentration of CT DNA in base pairs. The apparent absorption coefficients ϵ_a , ϵ_f , and ϵ_b correspond to $A_{\text{obs}}/[M]$, the extinction coefficient for the free metal(II) complex, and the extinction coefficient for the metal(II) complex in the fully bound form, respectively [50]. K_b is given by the ratio of the slope to the intercept.

Cyclic voltammetry and differential pulse voltammogram studies were performed on a CHI 620C electrochemical analyzer with a three-electrode system comprising glassy carbon as the working electrode, a platinum wire as the auxiliary electrode, and Ag/AgCl as the reference electrode. Solutions were deoxygenated by purging with N₂ prior to measurements.

Viscosity experiments were carried out on an Ostwald viscometer immersed in a thermostated water bath maintained at a constant temperature of 30.0 \pm 0.1 $^{\circ}$ C. CT DNA samples of approximately 0.5 mM were prepared by sonicating in order to minimize complexities arising from CT DNA flexibility [51]. The flow time was measured with a digital stopwatch three times for each sample, and an average flow time was then calculated. Data are presented as $(\eta/\eta_0)^{1/3}$ versus the concentration of the metal(II) complex, where η is the viscosity of the CT DNA solution in

the presence of the complex, and η_0 is the viscosity of the CT DNA solution in the absence of the complex. Viscosity values were calculated after correcting the flow time of the buffer alone (t_0), $\eta = (t - t_0)/t_0$ [52].

The degree of cleavage of the supercoiled (SC) pUC19 DNA (33.3 μM , 0.2 μg) to its nicked circular (NC) form was determined by agarose gel electrophoresis in 5 mM Tris–HCl buffer (pH 7.2) containing 50 mM NaCl. After they had been incubated for 2 h at 37 °C in a dark chamber, the samples were added to a loading buffer containing 25 % bromophenol blue, 0.25 % xylene cyanol, and 30 % glycerol (3 mm^3), and the solution was finally loaded onto 0.8 % agarose gel containing 1 $\mu\text{g}/\text{cm}^3$ ethidium bromide. Electrophoresis was carried out in a dark chamber for 3 h at 50 V in Tris–HCl–EDTA buffer. Bands were visualized by UV light and photographed.

Antimicrobial activity

The in vitro biological screening effects of the investigated compounds were tested against the Gram-positive bacteria *Staphylococcus aureus* and *Bacillus subtilis* and the Gram-negative bacteria *Escherichia coli* and *Klebsiella pneumoniae* by the well diffusion method [53], using agar nutrient as the medium and streptomycin as the standard. The antifungal activities of the compounds against the fungi *Aspergillus niger*, *Fusarium solani*, *Curvularia lunata*, and *Rhizoctonia bataicola* (cultured on potato dextrose agar as medium, and with nystatin used as the standard) were evaluated by the well diffusion method. The stock solution (10^{-2} M) was prepared by dissolving the compounds in DMSO, and the solutions were serially diluted in order to determine the minimum inhibitory concentration (MIC) values. In a typical procedure [54], a well was made in the agar medium inoculated with microorganisms. The well was filled with the test solution using a micropipette, and the plate was incubated for 24 h for bacteria and for 72 h for fungi at 35 °C. During this period, the test solution diffused and the growth of the inoculated microorganisms was affected. The inhibition zone developed, and the corresponding concentration was noted.

Molecular modeling studies

The interactions of the metal complexes with DNA were also studied by molecular modeling and docking. All calculations were performed in Open Eye with fast rigid exhaustive docking using the FRED docking software package. The main function employed for the calculations was ChemGauss 2. Prior to docking, the structures of the metal complexes were constructed and their geometries were optimized by the MM2 force field. The crystal

structure of the complex of netropsin with B-DNA dodecamer d(CGCGAATTCGCG)₂ (NDB code GDLB05) was downloaded from the Protein Data Bank. During the docking analysis, the binding site of netropsin was used as the binding site for our metal complexes across the entire DNA molecule. The docked poses were generated by the exhaustive search and optimization step. FRED selects the single best pose from among a set of candidates. This pose is then scored and the score is used to rank ligands in the output hit list. The consensus structure step allows multiple scoring functions to vote for the best docked structure in a rank-by-vote approach.

Statistical analysis

All of the experiments conducted in this work were done in triplicate, and all of the data are reported here as the mean \pm standard deviation.

Acknowledgments The authors express their sincere thanks to the Managing Board, the Principal, and the Head of the Department of Chemistry for providing research facilities and moral support. AS thanks the University Grants Commission (UGC) in Hyderabad for financial support.

References

1. Belaid S, Laandreau A, Djebbar S, Benail-Bouchara O (2008) J Inorg Biochem 102:63
2. Patil M, Hunoor R, Gudasi K (2010) Eur J Med Chem 45:2981
3. Liu YJ, Wang N, Mei WJ, Chen F, He LX, Jian LQ, Wang RJ (2007) Transition Met Chem 32:332
4. Vijayalakshmi R, Kanthimathi M, Subramanian V, Nair BU (2000) Biochim Biophys Acta 1475:157
5. Kasprzak KS (1991) Chem Res Toxicol 4:604
6. Raman N, Jeyamurugan R, Rajkapoor B, Mahesh V (2009) Appl Organometal Chem 23:283
7. Zeitsch KJ (2000) The chemistry and technology of furfural and its many by-products, 1st edn. Elsevier, Amsterdam, p 327
8. Stubbe J, Kozarich JW (1987) Chem Rev 87:1107
9. Pratviel G, Bernadou J, Meunier B (1995) Angew Chem Int Ed 34:746
10. Burrows CJ, Muller JG (1998) Chem Rev 98:1109
11. Sissi C, Mancin F, Gatos M, Palumbo M, Tecilla P, Tonellato U (2005) Inorg Chem 44:2111
12. Frey ST, Sun HHJ, Murthy NN, Karlin KD (1996) Inorg Chim Acta 242:329
13. Ranford JD, Sadler PJ, Tocher DA (1993) J Chem Soc Dalton Trans 3393
14. Mamedov VA, Kalinin AA, Azancheev NM, Levin YA (2003) Russ J Org Chem 39:125
15. Selvakumar PM, Suresh E, Subramanian PS (2007) Polyhedron 26:749
16. Bareefield EK, Freeman GM, Van Derveer DG (1986) Inorg Chem 25:552
17. Devries N, Reedijk J (1990) Inorg Chem 30:3700
18. Raman N, Sobha S (2012) Spectrochim Acta A 85:223
19. Nakamoto K (1970) Infrared spectra of inorganic and coordination compounds, 2nd edn. Wiley, New York

20. Lever ABP (1968) *Inorganic electronic spectroscopy*, 2nd edn. Elsevier, New York
21. Cotton FA, Wilkinson G (1988) *Advanced inorganic chemistry*, 5th edn. Wiley, New York
22. Konstantinovic SS, Radovanovic BC, Krkljes A (2007) *J Therm Anal Calorim* 90:525
23. Roy S, Mandal TN, Barik AK, Gupta S, Butcher RJ, Nethaji M, Kar SK (2008) *Polyhedron* 27:593
24. Raman N, Pothiraj K, Baskaran T (2011) *J Mol Struct* 1000:135
25. Prasad Singh V, Katiyar A (2008) *Pestic Biochem Phys* 92:8
26. Speier G, Csihony J, Whalen AM, Pierpont CG (1996) *Inorg Chem* 35:3519
27. Hathaway BJ, Bardley JN, Gillard RD (eds) (1971) *Essays in chemistry*. Academic, New York
28. Sitlani AS, Long EC, Pyle AM, Barton JK (1992) *J Am Chem Soc* 114:2303
29. Tysoe SA, Morgan RJ, Barker AD, Streckas TC (1993) *J Phys Chem* 97:1707
30. Kelly TM, Tossi AB, McConnell DJ, Oh Uigin C (1985) *Nucleic Acid Res* 13:6017
31. Pyle AM, Rehmman JP, Meshoyrer R, Kumar CV, Turro NJ, Barton JK (1989) *J Am Chem Soc* 111:3051
32. Li QG, Wang HM, Li AZ (1992) *Molecular biophysical chemistry*. Higher Education, Beijing (in Chinese)
33. Garnovskii AD, Nivorozkhin AL, Minkin VI (1993) *Coord Chem Rev* 126:1
34. Shahabadi N, Kashanian S, Darabi F (2010) *Eur J Med Chem* 45:4239
35. Chitrapriya N, Mahalingam V, Zeller M, Natarajan K (2010) *Inorg Chim Acta* 363:3685
36. Norden B, Tjerneld T (1982) *Biopolymers* 21:1713
37. Peng B, Chen X, Du KJ, Leyu B, Chao H, Nianji L (2009) *Spectrochim Acta A* 74:896
38. Ramakrishnan S, Palaniandavar M (2005) *J Chem Sci* 117:179
39. Tweedy BG (1964) *Phytopathology* 55:910
40. Raman N, Sakthivel A, Rajasekaran K (2009) *J Coord Chem* 62:1661
41. Sigel H (1973) *Metal ions in biological systems*, vol 2. Marcel Dekker, New York
42. Senthil Kumar R, Sasikala K, Arunachalam S (2008) *Inorg Biochem* 102:234
43. Panchal PK, Parekh HM, Pansuriya PB (2006) *J Enz Inhib Med Chem* 21:203
44. Perrin DD, Armarego WLF, Perrin DR (1980) *Purification of laboratory chemicals*. Pergamon, Oxford
45. Angllici RJ (1969) *Synthesis and techniques in inorganic chemistry*. WB Saunders, Philadelphia
46. Vogel AI (1989) *Text book of quantitative chemical analysis*, 5th edn. Longman, London
47. Ismail KZ, El-Dissouky A, Sheehada AZ (1997) *Polyhedron* 17:2909
48. Wolfe A, Shimer GH, Meehan T (1987) *Biochemistry* 26:6392
49. Reichmann ME, Rice SA, Thomas CA, Doty P (1954) *J Am Chem Soc* 76:3047
50. Tan LF, Liu XH, Chao H, Ji LN (2007) *J Inorg Biochem* 101:56
51. Charies JB, Dattagupta N, Cromers DM (1982) *Biochemistry* 21:3933
52. Satyanarayanan S, Davorusak JC, Charies JB (1983) *Biochemistry* 32:2573
53. Boyd RF (1988) *General microbiology*, 2nd int edn. Times Mirror/Mosby College, St. Louis
54. Kannan N (1996) *Laboratory manual in general microbiology*, 1st edn. Palani Paramount, Palani